*This research was supported by the U. S. Atomic Energy Commission under Contract No. AT(11-1)-GEN-10, P. A. 11.

[1]E. Østgaard, Phys. Rev. 170, 257 (1968).
[2]E. Østgaard, Phys. Rev. 171, 248 (1968).
[3]E. Østgaard, Phys. Rev. 176, 351 (1968).
[4]K. A. Brueckner and J. L. Gammel, Phys. Rev. 109, 1040 (1958); 121, 1863 (1961).
[5]M. Kirson, Nucl. Phys. A99, 353 (1967).
[6]L. M. Bruch and I. J. McGee, J. Chem. Phys. 46, 2959 (1967).
[7]W. R. Abel, A. C. Anderson, W. C. Black, and J. C. Wheatley, Phys. Rev. Letters 15, 875 (1965).
[8]N. M. Hugenholtz and L. Van Hove, Physica 24, 363 (1958).
[9]K. A. Brueckner and D. T. Goldman, Phys. Rev. 117, 207 (1960).
[10]K. A. Brueckner, S. A. Coon, and J. Dabrowski, Phys. Rev. 168, 1184 (1968).
[11]A. A. Abrikosov and I. M. Khalatnikov, Rept. Progr. Phys. 22, 329 (1959).
[12]D. Hone, Phys. Rev. 121, 669, 1864 (1961).
[13]V. J. Emery, Ann. Phys. (N. Y.) 28, 1 (1964).
[14]L. J. Campbell, Phys. Rev. 160, 236 (1967).
[15]G. Baym and C. Ebner, Phys. Rev. 170, 346 (1968).
[16]G. A. Brooker and J. Sykes, Phys. Rev. Letters 21, 279 (1968).
[17]V. J. Emery and D. Cheng, Phys. Rev. Letters 21, 533 (1968).
[18]H. Højgård Jensen, H. Smith, and J. W. Wilkins, Phys. Letters 27A, 532 (1968).
[19]J. C. Wheatley, Phys. Rev. 165, 304 (1968).
[20]H.-T. Tan and E. Feenberg, Phys. Rev. 176, 370 (1968).
[21]L. P. Pitaevskii, Zh. Eksperim. i Teor. Fiz. 37, 1794 (1959) [English transl.: Soviet Phys. – JETP 10, 1267 (1960)].
[22]L. P. Gorkov and L. P. Pitaevskii, Zh. Eksperim. i Teor. Fiz. 42, 600 (1962) [English transl.: Soviet Phys. – JETP 15, 417 (1962)].

PHYSICAL REVIEW VOLUME 180, NUMBER 1 5 APRIL 1969

Electronic Properties of Negative Ions in Liquid Helium*

B. DuVall† and V. Celli
Department of Physics, University of Virginia, Charlottesville, Virginia
(Received 23 December 1968)

The electronic properties of a negative ion in liquid He^4 are investigated theoretically. It is assumed that the ion consists of an electron trapped in a bubble, represented by a square-well potential of depth ~1 eV. Explicit analytic formulae are obtained which are useful for computing many properties of such an electron, including direct optical absorption and scattering of light accompanied by $1s$–ns and $1s$–nd transitions. Numerical values are given for the strength of $1s$–$1p$ transitions and for the scattering cross sections of laser light due to $1s$–$2s$ and $1s$–$1d$ transitions. The splitting of the $1p$ state due to the Jahn-Teller effect is investigated in detail, and the linewidths for the scattering processes are estimated.

I. INTRODUCTION

Ions in liquid helium have been the subject of considerable experimental and theoretical work since observations of their mobility were first reported by Careri and his group,[1] and theoretical models were developed by Atkins,[2] Kuper,[3] and others. It is now commonly agreed that the lowest energy configuration for a negative ion in liquid helium can be described as an electron trapped in a spherical bubble of radius 10 to 20 Å. The creation of this bubble is a consequence of the short-range repulsion between the electron and the helium atoms, due to the exclusion principle. This repulsion more than overcomes the long-range polarization of the surrounding fluid by the electron's charge. This model explains reasonably well the experimental low-field mobility and the trapping of the ions by vortices in rotating helium.[4]

Experiments have shown that there exists an energy barrier of about 1.0 eV for penetration of an electron into liquid helium.[5,6] A group at the University of Chicago has done extensive calculations based on the bubble model.[7,8] They have shown that an adequate model of the bubble is to treat it as an electron trapped in a square well. To obtain the total energy of the ion, the surface

energy of the bubble and a pressure-volume term must be added. Since the experimental work indicates a radius much larger than atomic dimensions one can disregard surface irregularities without appreciable error. Theoretical work[7–9] has also shown that the wall of the bubble is very sharp.

The bubble model predicts the existence of several excited states for the trapped electron, and these can in principle be detected by optical experiments. Northby and Sanders[10] and Zipfel and Sanders[11] have reported results of photoejection experiments. Other experiments such as optical absorption and Raman scattering have been planned. A major difficulty of course is the very low density of negative ions that can be obtained ($10^8/cm^3$ at present, but perhaps $10^{12}/cm^3$ in the foreseeable future). We present in this paper a thorough analytical treatment of the problem of an electron trapped in a square well of radius r_0 and finite depth V_0. This will give the necessary background theory for the interpretation of experimental data on optical properties of excess electrons in liquid helium. In view of the present uncertainty in the values of the parameters r_0 and V_0, the numerical examples we give are basically only indicative. In Sec. II, the theory of the excited states of the bubble is presented. The oscillator strengths and energy differences are calculated for the $1s$–np transitions. The configuration energy is computed to second order in the deformations for any state and also variationally for the $1p$ state, in connection with the Jahn-Teller effect. In Sec. III, the differential cross section for the Raman scattering is calculated. A rough estimate of the expected linewidth is given. A more detailed theory of the line shape, both for optical absorption and Raman scattering, is left for the time when, if ever, these experiments will be carried out. A preliminary report of some results contained in this paper was given elsewhere.[12] The theory of photoejection, or absorption in the continuum, has been dealt with by other authors[13] and will not be repeated here. For the calculation of the deformations and some of the formalism, we draw from a paper by Celli, Cohen, and Zuckermann,[14] to be referred to hereafter as CCZ.

During the preparation of this manuscript we learned of work by Fowler and Dexter[15] dealing with the optical properties of the electron bubble in helium. Unlike ours, the approach of these authors to the problem is by numerical techniques. In any event, we reduced duplication by keeping to a minimum our treatment of straight optical absorption, which is dealt with fairly exhaustively by these authors.

II. EXCITED STATES

In the spirit of the Born-Oppenheimer approximation, we consider the configuration coordinates to be fixed and solve for the electronic energy as a function of these coordinates.

Underformed Bubble

First of all we must find the eigenstates of the electron in a spherical bubble as a function of the radius r_0 and of the depth of the potential well V_0. This is a basic problem of quantum mechanics. The bound states will be labeled by the usual three quantum numbers n, l, m. The wave functions are of the form

$$r^{-1}R_{nl}(r)Y_{lm}(\theta,\phi), \quad \text{with } R_{nl}(r)=rN_{\text{in}}j_l(\alpha_{nl}r) \text{ for } r<r_0 ,$$

$$\text{and } R_{nl}(r)=rN_{\text{out}}h_l(\beta_{nl}r) \text{ for } r>r_0 .$$

The relation between α, β and the energy E is (in units such that $\hbar=1$),

$$\alpha^2=2m(V_0+E), \quad \beta=i(2m|E|)^{1/2} \text{ for } E<0, \quad \beta=(2mE)^{1/2} \text{ for } E>0 . \tag{2.1}$$

The energy eigenvalues E_{nl} are determined by (2.1) and the matching condition

$$W_l(E)=0 , \tag{2.2}$$

$$\text{where } W_l(E)=h_l'(\beta r_0)/h_l(\beta r_0)-j_l'(\alpha r_0)/j_l(\alpha r_0) . \tag{2.3}$$

Here and in the following a prime denotes differentiation with respect to r.

The normalization constants N_{in} and N_{out} are determined with the help of the standard integral[16]

$$I_l=\int u_l(ar)v_l(br)r^2dr=[r^2/(a^2-b^2)][bu_l(ar)v_{l-1}(br)-au_{l-1}(ar)v_l(br)] , \tag{2.4}$$

where the functions u_l and v_l can be any linear combination of spherical Bessel (or Hankel) functions of order l, with coefficients independent of l and of the argument.

Instead of N_{in} and N_{out}, we give an explicit form for the normalized radial wave function at the boundary of the well

$$R_{nl}(r_0) = (2/r_0)^{1/2}\beta_{nl}(\alpha_{nl}^2+\beta_{nl}^2)^{-1/2}[j_l'(\alpha_{nl}r_0)/j_l(\alpha_{nl}r_0)]$$
$$\times[j_l'(\alpha_{nl}r_0)/j_l(\alpha_{nl}r_0)+1/(\alpha_{nl}r_0)-l(l+1)/(\alpha_{nl}r_0)^2]^{-1/2} \quad . \tag{2.5}$$

Effect of Deformations

For a deformed bubble the potential energy of the trapped electron becomes

$$-V_0 S(r-r_0-\textstyle\sum_\lambda a_\lambda P_\lambda(\cos\theta)), \quad \text{where } S(x)=0 \text{ for } x>0, \quad S(x)=1 \text{ for } x<0 \quad . \tag{2.6}$$

The sum over λ can run from 0 to ∞, or from 1 to ∞, the term $\lambda=0$ being included in r_0. The deformation (2.6) is general enough for s states but for states of higher angular momentum one should include all spherical harmonics $Y_{\lambda\mu}$ in the expansion and not just the $Y_{\lambda 0}$ as in (2.6). However this considerably complicates the treatment, and we will not need the general case for the purposes of this paper. The energy of the trapped electron to second order in a_λ, with inclusion of surface energy and pressure terms, has been obtained by Celli, Cohen and Zuckerman[14] for the ground state of the electron bubble. By a completely analogous calculation we obtain for any bound state

$$E_{nlm}^{\text{tot}} = E_{nl}+4\pi\sigma r_0^2+(4\pi/3)pr_0^3+\textstyle\sum_\lambda S_{nlm}^\lambda a_\lambda+\frac{1}{2}\sum_{\lambda\lambda'}K_{nlm}^{\lambda\lambda'}a_\lambda^* a_{\lambda'} \quad , \tag{2.7}$$

where σ is the surface tension coefficient, p the external pressure and

$$S_{nlm}^\lambda = (8\pi\sigma r_0+4\pi p r_0^2)\delta_{\lambda 0}-V_0 R_{nl}^2(lm|P_\lambda|lm) \quad , \tag{2.8}$$

$$K_{nlm}^{\lambda\lambda'} = \delta_{\lambda\lambda'}[4\pi\sigma(\lambda^2+\lambda+2)+8\pi p r_0]/(2\lambda+1)-2V_0 R_{nl}R_{nl}'(lm|P_\lambda P_{\lambda'}|lm)$$
$$-2V_0^2 R_{nl}^2 r_0^2\textstyle\sum_{l'}\tilde{G}_{l'}(E_{nl})(l'm|P_\lambda|lm)(lm|P_{\lambda'}|l'm) \quad . \tag{2.9}$$

The matrix elements denote angular integrals over spherical harmonics. Their values are given in textbooks.[17] Here and in the following R_{nl} and R_{nl}' are respectively the radial wave function and its derivative with respect to r, evaluated at $r=r_0$. $\tilde{G}_{l'}(E_{nl})$ is related to the radial coefficient of the l'th spherical harmonics in the expansion of the Green's function for a spherical well, at energy E,

$$G_{l'}(r,r';E) = \textstyle\sum_{n'} R_{n'l'}(r)R_{n'l'}(r)/rr'(E_{n'l'}-E) \quad . \tag{2.10}$$

The relation is

$$\tilde{G}_{l'}(E_{nl}) = G_{l'}(r_0,r_0;E_{nl}) \quad , \quad \text{for } l\neq l' \quad , \tag{2.11}$$

$$\tilde{G}_l(E_{nl}) = \lim[G_l(r_0,r_0;E_{nl})-R_{nl}^2(r_0)/r^2(E_{nl}-E)], \text{ as } E\to E_{nl} \quad . \tag{2.12}$$

G_l is given explicitly in Sec. III. All we need here is the especially simple result

$$G_l(r_0,r_0;E) = -2m/r_0^2 W_l(E) \quad , \tag{2.13}$$

where W_l is given by (2.3). From (2.13) and the definition (2.10) it also follows that

$$R_{nl}^2(r_0) = 2m[(dW_l/dE)^{-1}]_{E=E_{nl}} \quad , \tag{2.14}$$

and, from (2.12)

$$\tilde{G}_l(E_{nl}) = (m/r_0^2)[(l^2 W_l/dE^2)/(dW_l/dE)^2]_{E=E_{nl}} \quad . \tag{2.15}$$

In general for computational purposes $W_l(E)$ is a very convenient quantity. Its zeros determine the energy eigenvalues, $W_l(E)$ itself is essentially the inverse of the Green's function which appears in (2.9) and in later formulas, and the derivatives of $W_l(E)$ at the zeros, which can be computed numerically at the same time as W_l, give the other interesting quantities (2.14) and (2.15). It is now a straightforward mat-

ter to compute the configurational energy diagrams up to second order in the deformations. Useful relations between $\tilde{G}$ and the wavefunctions R_{nl} can be obtained by looking in particular at the terms with $\lambda = 0$ and $\lambda = 1$ in (2.7). For the breathing mode $\lambda = 0$, one can alternatively obtain S and K by simply differentiating (2.7) with respect to r_0. Comparing the result with (2.8) and (2.9) one finds the following formulas, which are useful in the limit $V_0 \to \infty$:

$$dE_{nl}/dr_0 = -V_0 R_{nl}^2(r_0) \ , \tag{2.16}$$

$$d^2E_{nl}/dr_0^2 = -V_0 dR_{nl}^2/dr_0 = -2V_0 R_{nl}R_{nl}' - 2V_0^2 R_{nl}^2 r_0^2 \tilde{G}_l(E_{nl}) \ . \tag{2.17}$$

The last equality also follows from (2.14), (2.15), and (2.16). For the proper understanding of (2.17), we emphasize that $R_{nl}(r_0)$ is both an explicit and an implicit function of r_0 (through E_{nl}). We also remark that the equilibrium radius for each electronic state is determined by the condition

$$S^0_{lmn} = 0 \ . \tag{2.18}$$

One can also get useful relations from the fact that the $\lambda = 1$ mode is identical to first order to a rigid translation of the bubble, which must leave the energy unchanged. However, these relations are obtained more simply from the identity between matrix elements

$$(\vec{p})_{n'l'm',nlm} = -i(\vec{\nabla}V)_{n'l'm',nlm}/(E_{n'l'} - E_{nl}) \ . \tag{2.19}$$

We take for instance the z component, multiply both sides by $\chi_{n'l'} = R_{n'l'}/r$, sum over n', use completeness and the definition of $G_{l'}(E_{nl})$ and find

$$[\chi'(r) - V_0 G_{l'}(rr_0; E_{nl})](l'0|\cos\theta|l0) + [\chi(r)/r](l'0|\sin\theta\, \partial/\partial\theta|l0) = 0 \ . \tag{2.20}$$

The angular integrals are given in textbooks.[17] The great usefulness of (2.19) in this problem comes from the fact that $\vec{\nabla}V$ is proportional to a delta function $\delta(r - r_0)$.

Optical Absorption

As an application of the previous formulas, we have computed the energy difference between the ground state and the p states for typical values of the radius and V_0. The criteria used in selecting these values of r_0 and V_0 are discussed in Sec. III under the heading "Numerical values of the cross-sections." The results are reported in Table I, together with the values of the oscillator strengths for optical transitions from the ground state to the $1p$ state. The $2p$ and higher states have much smaller cross sections, as can be deduced from the fact that the $1p$ absorption almost exhausts the sum rule. These cross-sections are most simply computed[18] from the modulus square of the matrix element $(p_z)_{100,nlm}$ which is seen to be equal to

$$(\tfrac{1}{3})^{1/2} R_{1s}(r_0) R_{np}(r_0) V_0/(E_{np} - E_{1s})$$

by (2.19). An equivalent result is obtained by computing the matrix element $(z)_{100,nlm}$ with the help of the integral (3.13) of next section.

Similar results have been obtained by Fowler and Dexter[15] by numerical methods, but for somewhat different values of the radius. These authors also give an estimate of the absorption line width and discuss the feasibility of various experiments.

TABLE I. Optical-dipole-transition energies $E_{1p}-E_{1s}$ and $E_{2p}-E_{1s}$, oscillator strength for $1s$-$1p$ dipole transitions f_{1p}, linear and quadratic coefficients of the electronic energy of the $1p$ state for quadrupolar distortions, as a function of the bubble radius r_0 and depth V_0. The quantity S^d_{1p1} is the dimensionless quantity, $-2m\hbar^{-2}r_0^3 V_0 R_{11}^2 (11|P_2|11)$ [compare (2.8)]. For the $m=0$ state, $S^2_{110} = -2S^2_{111}$. K^d_{1p0} and K^d_{1p1} are also dimensionless quantities, related to K^{22}_{110} and K^{22}_{111} as defined in (2.9) by $K^{22}_{11} = (\hbar^2/2mr_0^4)K^d_{1p} + (8\pi/5)(4\sigma + pr_0)$.

r_0 (Å)	V_0 eV)	$E_{1p}-E_{1s}$ (eV)	$E_{2p}-E_{1s}$ (eV)	$10f_{1p}$	S^d_{1p1}	K^d_{1p0}	K^d_{1p1}
21	1.0	0.0742	0.3542	9.684	6.124	18.19	3.881
16	1.1	0.1219	0.5740	9.699	5.694	15.45	5.306
10	1.3	0.2772	not bound	9.763	4.728	9.805	2.796
16	0.7	0.1146	0.5181	9.728	5.170	12.30	3.881

Jahn-Teller Effect

We have performed rather detailed calculations of the configuration diagram for the $1p$ state, allowing both a radial deformation and a quadrupolar distortion. The latter separates the $m=0$ level from the $m=\pm 1$ levels. Formulas (2.8) and (2.9) allow us to draw the configuration energy diagrams to second order in the deformation parameters. All we need are explicit formulas for the angular integrals. For $\lambda=\lambda'=0$ they all reduce to unity and in fact formulas (2.16) and (2.17) can be used to advantage. For $\lambda=2$ the value of S is given by Feenberg and Hammack,[19] the eccentricity e being equal to $-\frac{3}{2}(a_2/r_0)$. Their result agrees with (2.8), with

$$(lm|P_2|lm)=[l(l+1)-3m^2]/(2l+3)(2l-1) \quad . \tag{2.21}$$

K[22] is given by Moszkowski[20] for an infinite well. Our more general result agrees in the limit $V_0\to\infty$, when the difference between a quadrupolar distortion and a spheroidal distortion is taken into account. The relevant angular integrals for p states are

$$(10|P_2^2|10)=\tfrac{11}{35}$$
$$(3m|P_2|1m)=(-1)^m\tfrac{1}{10}[\tfrac{3}{7}(3+m)\times(3-m)(2+m)(2-m)]^{1/2} \quad . \tag{2.22}$$

In practice the energy eigenvalues are given to a good approximation by the formula[20]

$$E_{nl}=\frac{x_{nl}^2}{2mR_0^2}\left(1-\frac{\lambda_0^3[x_{nl}^2-l(l+1)]}{1+\lambda_0}\right), \tag{2.23}$$

where x_{nl} is the nth zero of j_l and $\lambda_0=(2mV_0r_0^2)^{-1/2}$. With (2.23) as the initial guess, (2.3) is easily solved numerically to the desired accuracy. For completeness we record here some convenient explicity formulas:

$$r_0W_1(E)=-B^2/(1+B)-A^2/(1-C) \tag{2.24}$$

with $A=\alpha r_0$, $B=\beta r_0$, $C=A\cot A$;

$$\tfrac{1}{2}r_0R_{11}^2=\frac{A^2(1+B)^2}{(A^2+B^2)[B^2+3(1+B)]} \tag{2.25}$$

and $$\left[\frac{d^2W_1}{dE^2}\right]_{E=E_{nl}}=\frac{1}{4B}\frac{3+B}{(1+B)^3}-\frac{1}{4(1-C)^3}$$
$$\times[(3C/A^2)(1-C)^2-(5+2C)(1-C)+2A^2] \quad . \tag{2.26}$$

Finally,

$$r_0W_3(E)=-B^2/(5+B^2D)-A^2/(5-A^2D) \tag{2.27}$$

with $D=(1+B)/(3+3B+B^2)$.

Formulae (2.21) through (2.27) allow explicit computation of S and K for $\lambda=0, 2$ and $p=1$, $m=0$ and ± 1. Indicative results are displayed in Table I in the last three columns.

We have also used a variational approach to determine the shape and the energy of the $1p$ level. If the surface of the bubble is given by

$$R(\theta)=r_0(1+a_2'P_2+\cdots) \tag{2.28}$$

a good variational wave function for the limiting case of $V_0\to\infty$ is, apart from normalization,

$$\psi=j_1(\alpha r/R(\theta))Y_1^m(\theta,\phi) \quad . \tag{2.29}$$

Since ψ must vanish at the surface, $j_1(\alpha)=0$. The electronic energy will be the expectation value of the kinetic energy operator. The total energy, which is to be minimized with respect to the variational parameters r_0, a_2', can be written in the form

$$E_t=\frac{F(a_2')}{r_0^2}+F_s(a_2')r_0^2+F_v(a_2')r_0^3 \quad .$$

Here F/r_0^2, $F_sr_0^2$, and $F_vr_0^3$ are the electronic, surface, and volume energy terms respectively. For the case of zero external pressure and $\sigma=0.5$ dyn/cm, the total energy of the $m=0$ state is found to be 0.327 eV with $r_0=19.9$ Å and $a_2'=0.347$, while for the $m=\pm 1$ states, the total energy is 0.342 eV, $r_0=20.6$ Å and $a_2'=-0.177$. If no relaxation were allowed, i.e., $a_2'=0$, then the minimization procedure gives $E_t=0.348$ and $r_0=21$ Å.

In Fig. 1 a plot of $F(a_2')$ is given and for comparison the results of perturbation theory are also drawn, both for the case $V_0\to\infty$ and for the representative value $V_0=1$. The surface and volume terms are trivial to compute and in fact they are well approximated by the second-order expressions which appear in (2.8) and (2.9).

In sum, the indication is that in the excited state the bubble deforms substantially, but not so much that perturbation theory becomes useless for quantitative estimates. In particular, we have further checked by an independent variational calculation that in the $m=\pm 1$ state the bubble does not deform all the way into a toroidal shape.

III. RAMAN SCATTERING

We consider here electronic Raman scattering, i.e., the process where an incoming photon of frequency ω_0 is absorbed, leaving the electron in an excited state, and a photon of frequency ω is emitted. Energy is also exchanged with the surrounding fluid through the boundary of the bubble, and this determines the linewidth and the line shape of each electronic Raman transition. In the Born-Oppenheimer approximation, the inte-

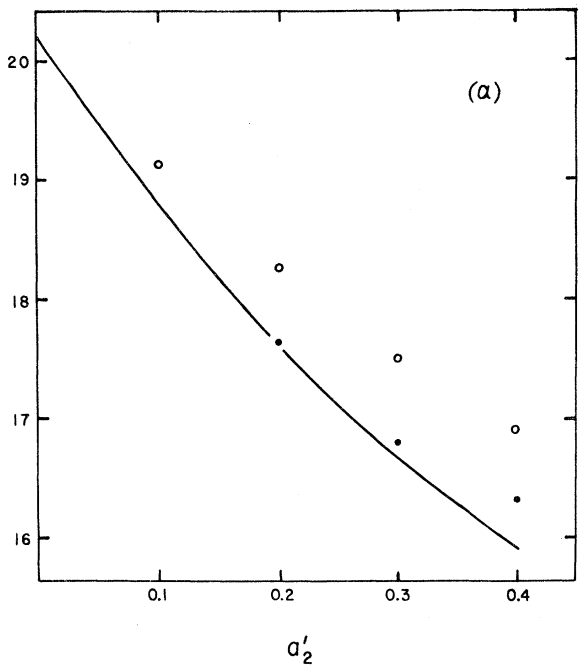

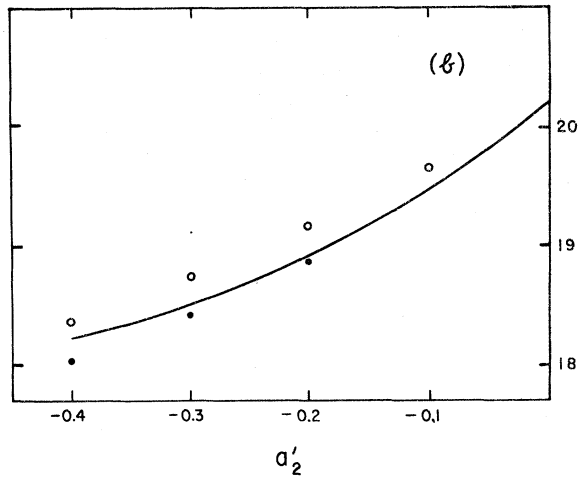

FIG. 1. Plot of the electron energy in units of $\hbar^2/2mr_0^2$ versus the dimensionless parameter of quadrupolar deformation for the $1p$ state with $m=0$ (a) and with $m=\pm 1$ (b). The solid line is the result of the variational calculation for a potential well of infinite depth, i.e., a plot of $(\hbar^2/2m)\,F(a_2')$, where F is defined in (2.30). The isolated points give for comparison the results of perturbation theory to second order in the deformation for a potential well of infinite depth (●) and for a well of depth 1 eV and radius 16 Å (○). For ease of display the energy scale for the ○ points has been shifted to make all energies coincide at zero deformation.

grated transition probability for a given line is computed for an undeformable bubble and a configuration-coordinate analysis is used for determining the effect of interactions with the motion of the boundary.

The Raman scattering cross section for a nonrelativistic free electron or an electron in a harmonic oscillator potential is zero. Therefore a rather careful calculation is necessary to see if the bubble model for the electron in liquid helium predicts an appreciable Raman scattering cross section. We assume the electron to be in a square well of finite depth.

In the usual dipole approximation, the differential cross section for scattering an incoming photon of frequency ω_0 and polarization vector $\vec{e}$ into a photon of frequency ω, polarization vector $\vec{e}'$ and propagation vector within the solid angle $d\Omega$ is given by[18]

$$d\sigma/d\Omega = r_e^{\,2}|M|^2\omega/\omega_0 \ . \tag{3.1}$$

The classical electron radius r_e is equal to e^2/mc^2, where m is the mass of the electron. The matrix element M is (in units such that $\hbar=1$)

$$M = m^{-1}\sum_i [(\vec{p}\cdot\vec{e})_{fi}(\vec{p}\cdot\vec{e}')_{i0}/(E_i - E_0 - \omega_0) + (\vec{p}\cdot\vec{e}')_{fi}(\vec{p}\cdot\vec{e})_{i0}/(E_i - E_0 + \omega)] \ . \tag{3.2}$$

Here, E and $\vec{p}$ are the electron energy and momentum, and the subscripts 0, f, and i refer to the ground, final, and intermediate states. Conservation of energy states that the scattered frequency ω is given by $\omega = \omega_0 + E_0 - E_f$.

If the electron is initially in the ground state, the final state must have angular momentum 0 or 2 for an allowed Raman transition to occur.

Green's-Function Method

The sum over the intermediate states in (3.2) can be performed by using the Green's function

$$G(\vec{r},\vec{r}';E) = \sum_l G_l(r,r';E)\, Y_l^{\,m}(\theta,\phi) Y_l^{*m}(\theta',\phi') \tag{3.3}$$

where G_l is given in (2.10), and satisfies the differential equation

$$\left[-\frac{1}{r^2}\frac{d}{dr}\left(r^2\frac{d}{dr}\right) + \frac{l(l+1)}{r^2} - 2mV_0 S(r-r_0) - 2mE\right] G_l(r,r') = \frac{2m}{r^2}\delta(r-r') \tag{3.4}$$

with the boundary conditions that $G_l(r,r')$ must be regular at $r=0$ and must have the asymptotic form of an outgoing wave. A finite linewidth Γ becomes important when one of the energy denominators vanishes

in the matrix element M, equation (3.2). The second term in M has no vanishing denominators. The first term, for the values of r_0, V_0, and ω_0 of interest, has vanishing denominators only in the continuum. Since the structure of the continuum is expected to be broad compared to the linewidth, taking the limit $\Gamma \to 0$ appears to be reasonable.

The explicit solution of (3.4) will now be displayed for the various regions of the variables r and r'. For compactness the subscript l is omitted in the notation, since G_l consists only of Bessel functions of order l. We use the definitions (2.1) for α and β and the convention that a prime denotes differentiation with respect to r. For $r < r'$ we obtain then, with $Z = j(\alpha r_0)h'(\beta r_0) - j'(\alpha r_0)h(\beta r_0)$,

$$G_l = -2m\alpha j(\alpha r)\{n(\alpha r') + j(\alpha r')[h(\beta r_0)n'(\alpha r_0) - h'(\beta r_0)n(\alpha r_0)]/Z\}, \quad \text{for } r < r' < r_0 , \tag{3.5}$$

$$G_l = -(2m/r_0^2)j(\alpha r)h(\beta r')/Z , \quad \text{for } r < r_0 < r' , \tag{3.6}$$

$$G_l = -2m\beta h(\beta r')\{j(\beta r)[j(\alpha r_0)n'(\beta r_0) - j'(\alpha r_0)n(\beta r_0)] + n(\beta r)[j'(\alpha r_0)j(\beta r_0) - j(\alpha r_0)j'(\beta r_0)]\}/Z , \quad \text{for } r_0 < r < r' . \tag{3.7}$$

For $r > r'$, the quantity G_l is obtained by interchanging r and r'. When $r = r_0$ and $r' = r_0$, G_l reduces to the simple form (2.13).

s–s Scattering Cross Sections

Now we use the Green's function to evaluate the scattering matrix element M. After letting the momentum operators in equation (3.2) act on the initial and final states, each of the angular integrations is simply a product of two spherical harmonics. Only the $l = 1$ term in the expansion for G[Eq. (3.3)] does not integrate to zero. The result of the angular integrations when the final state has s symmetry is $\vec{e} \cdot \vec{e}'/3$. The remaining radial integrals must be divided into the various regions of $G_1(r, r')$. The process is lengthy, but all integrals are of the standard form (2.4). The final result for the radial part of the matrix element is written conveniently in terms of the radial wave function

$$\chi_{nl}(r) = R_{nl}(r)/r \tag{3.8}$$

and its derivative $\chi_{nl}'(r)$, evaluated at $r = r_0$:

$$M_{\text{rad}}^{0-0} = (V_0 r_0^2 \chi_{10}\chi_{n0}/m\omega\omega_0)\{\chi_{10}'/\chi_{10} + \chi_{n0}'/\chi_{n0} + V_0 r_0^2[G_1(r_0, r_0; E_0 + \omega_0) + G_1(r_0, r_0; E_0 - \omega)]\}. \tag{3.9}$$

In turn R_{nl} is given by (2.5), (2.14), or (2.16), whichever is most convenient, and G_1 is given by (2.13).

An alternative formula for M can be obtained most simply by converting the matrix elements of $\vec{p}$ in (3.2) with the help of (2.19). Then the product of three energy differences appears in the denominators. Splitting this into partial fractions we find for the radial part

$$M_{\text{rad}}^{0-l} = (V_0^2 r_0^4/m\omega\omega_0)\chi_{10}\chi_{nl}[G_1(E_{10} + \omega_0) + G_1(E_{10} - \omega) - G_1(E_{10}) - G_1(E_{nl})], \quad \text{for } l = 0, 2 . \tag{3.10}$$

The equivalence of (3.10) for $l = 0$ to (3.9) is easily seen with the help of (2.20) for $l = 0$, $l' = 1$, $r = r_0$. The cross section is then

$$d\sigma/d\Omega = r_e^2(\omega/\omega_0)|M_{\text{rad}}^{0-0}|^2(\vec{e} \cdot \vec{e}'/3)^2 . \tag{3.11}$$

Numerical values are given in a following subsection.

s–d Scattering Cross Sections

For the case of scattering from the $1s$ level to a d level it is convenient to change the form of the matrix element M in equation (3.2) so that it contains matrix elements of $\vec{r}$ instead of $\vec{p}$. This is accomplished by the relation $(\vec{p})_{ab} = im\omega_{ab}(\vec{r})_{ab}$ where $\omega_{ab} = E_a - E_b$. After algebraic manipulation, the matrix element becomes

$$M = m\omega\omega_0 \sum_i [(\vec{r} \cdot \vec{e})_{fi}(\vec{r} \cdot \vec{e}')_{i0}/(\omega_{i0} - \omega_0) + (\vec{r} \cdot \vec{e}')_{fi}(\vec{r} \cdot \vec{e})_{i0}/(\omega_{if} + \omega_0)] . \tag{3.12}$$

The same Green's function is used to evaluate the sum over the intermediate states. The result of the angular integrations depends on the azimuthal quantum number m of the final d state, while the radial integrals are the same for all values of m.

Again the range of radial integration must be broken into several regions. The integrals over r are of the type (2.4) and the remaining integrals over the variable r' are found to be of the type I_l of (2.4), of the type

$$J_l = \int u_{l-1}(ar) v_l (br) r^3 dr = (l+1) I_l/a + \partial I_l/\partial a \tag{3.13}$$

and of the type

$$\int u_{l-1}(ar) v_{l+1}(br) r^4 dr = l J_l/b - \partial J_l/\partial b \ . \tag{3.14}$$

The final result for the radial part of the matrix element is

$$M_{\text{rad}}^{0-2} = (\chi_{10}\chi_{n2} V_0 r_0^2/m\omega\omega_0)\{3/r_0 + \chi_{10}'/\chi_{10} + \chi_{n2}'/\chi_{n2} + V_0 r_0^2[G_1(r_0, r_0; E_0+\omega_0) + G_1(r_0, r_0; E_0-\omega)]\} \ . \tag{3.15}$$

The equivalence of (3.15) and (3.10) for $l=2$ can be shown by use of (2.20) for $l=2$, $l'=1$.

Summing the modulus square of the matrix element over all values of the azimuthal quantum number m in the final state and inserting in (3.1), we obtain

$$d\sigma/d\Omega = r_e^2(\omega/\omega_0)(M_{\text{rad}}^{0-2})^2[(\vec{e}\cdot\vec{e}')^2+3]/45 \ . \tag{3.16}$$

where M_{rad}^{0-2} is given by (3.15) or (3.10), whichever is more convenient.

Numerical Values of the Cross Sections

If the scattered photon is observed regardless of its polarization, we must sum over the possible values of $\vec{e}'$ in (3.11) and (3.16). The result for $s-s$ scattering is

$$d\sigma/d\Omega = r_e^2(\omega/\omega_0)|M_{\text{rad}}^{0-0}|^2 \tfrac{1}{9}\sin^2\theta \tag{3.17}$$

and for the $s-d$ scattering

$$d\sigma/d\Omega = r_e^2(\omega/\omega_0)|M_{\text{rad}}^{0-2}|^2 (6+\sin^2\theta)/45 \ , \tag{3.18}$$

where θ is the angle between $\vec{e}$ and $\vec{k}'$, i.e., between the polarization of the incoming photon and the direction of scattering.

To obtain numerical values for the cross section and the frequency shifts in scattering, we need to know r_0 and V_0. The radius r_0 can be regarded as a physical adjustable parameter, since it varies significantly with applied pressure. V_0 also varies slightly with pressure.

Using the model of an electron in a square well, Springett, Cohen, and Jortner[8] have been able to satisfactorily fit Springett's and Donnelly's[4] "experimental" values of the radius as a function of pressure. The pressure dependence of the surface tension was adjusted to fit the data, but it agrees reasonably well with predictions of Amit and Gross.[19] A considerably larger "experimental" radius is obtained by fitting Northby and Sander's photoconductivity data.[10] We display in Table II indicative values of the cross sections and energy shifts in the $1s-2s$ and $1s-2d$ transition for an incoming frequency $\hbar\omega_0 = 1.96$ eV (He – Ne laser). The values of r_0, V_0 in the first row are those given in Ref. 10; in the next two rows they are the "best" values from reference 8, at zero pressure and at the extreme pressure of 20 atm. In the last row we use a value of V_0 close to the one deduced from the most re-

TABLE II. Raman scattering cross sections and linewidth parameters. The values of the cross sections are evaluated at $\sin\theta = 1$. The cross sections and energy shifts have been calculated assuming that $\hbar\omega_0 = 1.96$ eV (He-Ne laser). The coefficients in the last two columns are necessary to compute the linewidths as given by (3.26) and (3.27).

r_0 (Å)	V_0 (eV)	$d\sigma/d\Omega$ $1s-2s$ (10^{-30} cm^2)	$E_{2s}-E_{1s}$ (eV)	$d\sigma/d\Omega$ $1s-1d$ (10^{-30} cm^2)	$E_{1d}-E_{1s}$ eV)	$V_0 R_{2s}^2 r_0$ (eV)	$V_0 R_{1d}^2 r_0$ (eV)
21	1.0	3.57	0.212	3.18	0.168	0.510	0.433
16	1.1	10.30	0.346	7.53	0.275	0.803	0.689
10	1.3	219.00	0.755	161.00	0.617	1.495	1.410
16	0.7	5.87	0.320	4.22	0.257	0.698	0.616

cent photoejection data,[11] which indicate a radius in agreement with previous estimates but a considerably shallower potential well.

The cross sections given in Table II are the peak values, i.e., they are computed from (3.1) and (3.18) for $\sin\theta = 1$. The change with pressure of the cross section appears to be considerable. While the absolute magnitudes of the cross sections are not easily measured, their relative magnitudes for various levels and the frequency shifts of the scattered radiation can provide a quantitative test of the bubble model. The analytical expressions that have been derived here can then be used to decide which values of the radius of the bubble r_0 and the depth of the potential V_0 give the best agreement with the experimental data.

The cross sections in Table II are of the same order of magnitude as the very strong 992 cm^{-1} Raman line of benzene. This line is a vibrational Raman effect and the cross section is of the order of magnitude of 10^{-29} cm^2 for an incident photon wavelength of 4880 Å.[22] The experimentally observed signal depends of course on the product of the cross section and the number of scattering centers. For excess electrons in helium, the density of scattering centers (bubbles) is typically 10^7–10^9 per cm^3, while in benzene there are about 10^{21} active centers (molecules) per cm^3. In order to make the signal marginally detectable, using available high power lasers and refined counting techniques, the effective ion density must be increased at least to 10^{12} per cm^3.

Approximate Calculations

Fomin[23] has estimated the $1s$–$1d$ cross section for an infinitely deep potential well of radius 19 Å, obtaining a value considerably larger than the $1s$–$1d$ cross sections given in Table II. The difference is due to the fact that instead of carrying out the sum over all the intermediate states, Fomin has kept only the contribution from the $1p$ state. This is a standard approximation in estimating Raman cross sections, but in this case it leads to a gross overestimate, since the $1p$ and $2p$ contributions are of opposite sign and almost cancel each other.

Since the matrix elements of $\vec{p}\cdot\vec{e}$ decrease fairly rapidly, one might expect that the sum of the first few terms gives a good approximation to the total. If the frequencies ω_0 and ω are much larger than the first few energy differences in the denominators of equation (3.2), one can expand in terms of ω_0^{-1} and use (2.19) to carry out the sum over intermediate states. Correct up to terms of the order ω_0^{-3}

$$M = (1/m\omega_0^2)[(\vec{e}\cdot\vec{\nabla})(\vec{e}'\cdot\vec{\nabla})V]_{f0} \quad . \tag{3.19}$$

This approximation should be valid for any potential $V(\vec{r})$ in the shape of a well, if the depth of the well is much less than ω_0. Thus it allows treatment of the case when $V(r)$ is not simply a square-well potential. If equation (3.19) is used to calculate the $1s$–$2s$ or the $1s$–$1d$ scattering for the square well, it gives the same answer as the exact formulas (3.9) and (3.15), except that the terms containing G_1 are omitted. For the values of the parameters that have been used in Table II, the results are not expected to be much better than an order of magnitude since $\omega_0 \simeq 2$ eV and $V_0 \simeq 1$ eV. In fact the results given by this approximation are within a factor of 3 of the results of the exact calculation.

Linewidth

We give here only a rough estimate of the linewidth for the Raman absorption line, for the purpose of guiding experimental work on this effect. If and when experiments are successfully carried out, a more detailed theory of the line shape will be in order.

We use the configuration energy diagrams, computed to second order by the formulae of Sec. I, and the Franck-Condon principle. The dominant contribution to the linewidth in this scheme comes from the deformations that alter the energy of the final state to first order. What can be computed easily is in fact the second moment of the line, which we can regard as the square of the linewidth W:

$$W^2 = \int(\omega - \bar{\omega})^2 F(\omega)d\omega / \int F(\omega)d\omega \quad , \tag{3.20}$$

where[24]

$$F(\omega) = \mathrm{av}[\textstyle\sum_f |M_{0f}(x)|^2 \delta(E_f(x) - E_0(x) - \omega)]. \tag{3.21}$$

Here $M_{0f}(x)$ is the matrix element (3.12) as a function of the distortion coordinates, indicated collectively by x; the quantity $\bar{\omega} = Ef(0) - E_0(0)$ is the center frequency of the line and $E_f(x)$ and $E_0(x)$ are the final- and ground-state energies as a function of the distortion coordinates. The average is taken over the values of x in the ground state. In our case the distortion coordinates are the $a_{\lambda\mu}$ of the expansion

$$r = r_0 + \textstyle\sum_{\lambda\mu} a_{\lambda\mu} Y_{\lambda\mu} \quad , \tag{3.22}$$

for the boundary of the bubble. The final states f are, for instance, the five degenerate $2d$ states. Because of the sum over all degenerate final states, it is not necessary to investigate how this degeneracy splits under the deformation, but we have simply

$$W^2 = V_0^2 R_{nl}^4 \sum_{mm'm''} \mathrm{av}(M_{0,nlm} D_{mm'} \times D_{m'm''} M^*_{0,nlm''}) / \textstyle\sum_m |M_{0,nlm}|^2, \tag{3.23}$$

where

$$D_{mm'} = (lm|\sum_{\lambda\mu} a_{\lambda\mu} Y_{\lambda\mu}|lm') \ . \qquad (3.24)$$

After taking the average, only terms proportional to $\mathrm{av}(|a_{\lambda\mu}|^2)$ remain, and in fact such ground state averages are independent of μ. We can then set $m'' = m$ and use the result[25]

$$\sum_{m'\mu} |(lm'|Y_{\lambda\mu}|lm)|^2 = \frac{(2l+1)(2\lambda+1)}{4\pi} \begin{pmatrix} l & \lambda & l \\ 0 & 0 & 0 \end{pmatrix}^2 , \qquad (3.25)$$

to completely evaluate W^2. The matrix elements M cancel out because (3.25) is independent of m. Using the tabulated values of the 3-j coefficients,[17] we get for $1s$–ns transitions

$$W_{s-s}^{\ 2} = V_0^{\ 2} R_{n0}^{\ 4} \mathrm{av}(a_0^{\ 2}) \ , \qquad (3.26)$$

(which could be derived more directly), and for $1s$–nd transitions

$$W_{sd}^{\ 2} = V_0^{\ 2} R_{n2}^{\ 4} \mathrm{av}[a_0^{\ 2} + \tfrac{2}{7}(a_2^{\ 2} + a_4^{\ 2})] \ . \qquad (3.27)$$

In (3.26) and (3.27) we have reverted to the coefficient a_λ of (2.6). Clearly $a_\lambda^{\ 2} = (2\lambda+1)a_{\lambda 0}^{\ 2}/4\pi$.

An evaluation of the averages as a function of temperature can be carried out by use of the theory given in CCZ. However, an order of magnitude guess is probably sufficient, since it is hard to see how the rms displacement of any a_λ could be much different from, say, $\frac{1}{100}$th of r_0 at temperatures around 1°K or higher.[15] These temperatures are high enough that each resonance in the vibration of the bubble boundary can be treated as a single classical oscillator of frequency about 10^{11} sec^{-1}, corresponding to an energy smaller than the thermal energy kT. Therefore we have

$$\mathrm{av}(a_\lambda^{\ 2}) \approx kT/K_{000}^{\lambda\lambda} \ . \qquad (3.28)$$

In the notation of CCZ, K_0 corresponds to K_{000}^{00} of this paper and $K_2/5$ is equal to K_{000}^{22}. We have not computed explicitly K_{000}^{44}, but it is hard to see how it could differ in magnitude from the other two coefficients. We have then explicitly in units of Å^2

$$\mathrm{av}(a_0^{\ 2}) = 1.38T/K_0 \ , \qquad (3.29)$$

where K_0 is given in Table I of CCZ in (erg/cm^2). An analogous formula holds for a_2. We see that the rms value of a_0 is typically 0.1 Å, or $\frac{1}{100}$th of r_0, hence $W_{s-s} \approx 0.01 T V_0 R_{n0}^{\ 2} r_0$.

With the help of Table II of CCZ we can estimate in a similar way $\frac{2}{7}\mathrm{av}(a_2^{\ 2})$ and find that it is of the same order as $\mathrm{av}(a_0^{\ 2})$. Assuming that $\frac{2}{7}\mathrm{av}(a_4^{\ 2})$ is also comparable in magnitude, we see that $W_{s-d} \lesssim 0.02 T V_0 R_{n2}^{\ 2} r_0$. The values of $V_0 R_{20}^{\ 2} r_0$ and $V_0 R_{12}^{\ 2} r_0$ are listed in the last two columns of Table II. The qualitative behavior of $V_0 R_{nl}^{\ 2} r_0$ as a function of the radius r_0 can be understood in the infinite-well limit. Then from (2.9) and (2.20) one can see that this quantity varies as r_0^{-2}, and this dependence is dominant even for a well of finite depth. We conclude that at 1°K, the quantity W_{s-s} is of the order of 0.01 eV and that W_{s-d} is probably less than 0.02 eV.

Comparing with the energy difference $E_{2s} - E_{1d}$, we see that the width of each line is always considerably smaller than its frequency and furthermore that the two lines corresponding to $1s$–$2s$ and $1s$–$1d$ transitions should be separable, if r_0 is smaller than the largest quoted value (21 Å).

ACKNOWLEDGMENTS

We are indebted to W. B. Fowler for sending us a copy of his paper with D. L. Dexter in advance of publication, and for a discussion of the estimate of the linewidth. The stimulus for this work was provided by discussions with B. Deaver and F. Moss.

---

*Supported by the Air Force Office of Scientific Research under grant/contract AFOSR-1138-66 and by the National Science Foundation.

†Based in part on a dissertation submitted for the partial fulfillment of the Ph. D. requirements at the University of Virginia, Charlottesville, Virginia.

[1]G. Careri, F. Scaramuzzi, and J. O. Thomson, Nuovo Cimento 13, 186 (1959).

[2]K. R. Atkins, Phys. Rev. 116, 1339 (1959).

[3]C. G. Kuper, Phys. Rev. 122, 1007 (1961).

[4]B. E. Springett and R. J. Donnelly, Phys. Rev. Letters 17, 364 (1966); for a recent discussion of the data see B. E. Springett and H. M. Randall, in "Proceedings of the Eleventh International Conference on Low-Temperature Physics, St. Andrews, Scotland, 1968" (to be published).

[5]W. T. Sommer, Phys. Rev. Letters 12, 271 (1964).

[6]Michael A. Woolf and G. W. Rayfield, Phys. Rev. Letters 15, 235 (1965).

[7]Joshua Jortner, Neil R. Kestner, Stuart A. Rice, and Morrel H. Cohen, J. Chem. Phys. 43, 2614 (1965); Kazuo Hiroike, Neil R. Kestner, Stuart A. Rice, and Joshua Jortner, J. Chem. Phys. 43, 2625 (1965).

[8]B. E. Springett, Morrel H. Cohen, and Joshua Jortner, Phys. Rev. 159, 183 (1967).

[9]R. C. Clark, Phys. Letters 16, 42 (1965).

[10]J. A. Northby and T. M. Sanders, Jr., Phys. Letters 18, 1184 (1967).

[11]C. Zipfel and T. M. Sanders, in "Proceedings of the Eleventh International Conference on Low-Temperature Physics, St. Andrews, Scotland, 1968" (to be published).
[12]B. Du Vall and V. Celli, Phys. Letters 26A, 524 (1968).
[13]S. Wang, Ph. D. thesis, University Of Michigan, 1967 (unpublished); I. A. Fomin, Zh. Eksperim. i Teor. Fiz – Pis'ma Redakt. 6, 373 (1967) [English transl.: JETP Letters 6, 760 (1967)].
[14]V. Celli, Morrel H. Cohen, and M. J. Zuckermann, Phys. Rev. 173, 253 (1968).
[15]W. B. Fowler and D. L. Dexter, to be published.
[16]Philip M. Morse and Herman Feshbach, Methods of Theoretical Physics (McGraw-Hill Book Company, Inc., New York, 1953), p. 1574.
[17]A. R. Edmonds, Angular Momentum in Quantum Mechanics (Princeton University Press, Princeton, New Jersey, 1957).
[18]W. Heitler, The Quantum Theory of Radiation, (Oxford University Press, London, 1954).
[19]E. Feenberg and K. C. Hammack, Phys. Rev. 81, 285 (1951).
[20]S. A. Moszkowski, Phys. Rev. 99, 803 (1955).
[21]D. Amit and E. P. Gross, Phys. Rev. 145, 130 (1966).
[22]J. G. Skinner and W. G. Nilsen, J. Opt. Soc. Am. 58, 113 (1968).
[23]I. A. Fomin, Zh. Eksperim. i Teor. Fiz – Pis'ma Redakt. 6, 715 (1967) [English transl.: JETP Letters 6, 196 (1967)].
[24]See, e.g., C. H. Henry, S.E. Schnatterly, and C.P. Slichter, Phys. Rev. 137, A583 (1965); see also Ref. 15.
[25]Manuel Rotenberg *et al.*, The 3-*j* and 6-*j* Symbols (Massachusetts Institute of Technology Press, Cambridge, Mass., 1959), p. 5.

PHYSICAL REVIEW VOLUME 180, NUMBER 1 5 APRIL 1969

Electron-Impact Broadening of Isolated Lines of Neutral Atoms in a Plasma. I*

J. Cooper
Joint Institute for Laboratory Astrophysics and Department of Physics and Astrophysics, University of Colorado, Boulder, Colorado
and
G. K. Oertel
National Aeronautics and Space Administration, Washington, D.C. 20546
(Received 21 June 1968)

This paper deals with the generalized impact theory for electron broadening of isolated spectral lines emitted by neutral atoms in a plasma. The existing theory is improved by quantitative evaluation of the second-order (quadrupole) term in the multipole expansion including broadening of the lower level and interference effects, by approximate inclusion of the "back reaction" of atom on perturber in inelastic collisions through symmetrization with respect to initial and final perturber states, and by corrections to the broadening functions in the classical-path approximation. While the quadrupole contribution is normally a small correction, it is shown that it may, in principle, dominate the weak collision broadening in some situations even when the multipole series converges; however, strong collisions will always dominate in this case. Numerical results of the improved theory are given for the half-widths at half-maximum of some helium I lines, and the effects of the corrections are evaluated.

I. INTRODUCTION

The modern theory of Stark broadening of isolated spectral lines is based upon the comprehensive paper by Griem, Kolb, Baranger, and Oertel[1] (GBKO). They give explicit expressions for the width and shift in terms of the S-matrix elements for an electron collision, and the same expressions are obtained by Cooper[2] using a density-matrix formulation of the impact approximation. The GBKO theory has proved highly successful in predicting widths and shifts of isolated lines of neutrals, especially helium.[3,4] However, experiments (first independently by Jalufka *et al.*[5] and Popenoe *et al.*[6]) showed that for ion lines the GBKO widths are often too small (by factors of